Catalysts **2015**, *5*, 2309-2323; doi:10.3390/catal5042309

OPEN ACCESS

catalysts

ISSN 2073-4344

www.mdpi.com/journal/catalysts

Article

Switching off H_2O_2 Decomposition during TS-1 Catalysed Epoxidation via Post-Synthetic Active Site Modification

Ceri Hammond * and Giulia Tarantino

Cardiff Catalysis Institute, School of Chemistry, Cardiff University, Cardiff CF10 3AT, UK;
E-Mail: tarantinog@cardiff.ac.uk

***** Author to whom correspondence should be addressed; E-Mail: hammondc4@cardiff.ac.uk;
Tel.: +44-29-2087-4082.

Academic Editor: Andreas Martin

Received: 28 October 2015 / Accepted: 16 December 2015 / Published: 21 December 2015

Abstract: Despite its widespread use, the Lewis acidic zeolite, TS-1, still exhibits several unfavourable properties, such as excessive H_2O_2 decomposition, which decrease its overall performance. In this manuscript, we demonstrate that post-synthetic modification of TS-1 with aqueous NH_4HF_2 leads to modifications in epoxidation catalysis, which both improves the levels of epoxide selectivity obtained, and drastically minimises undesirable H_2O_2 decomposition. Through *in situ* spectroscopic study with UV-resonance enhanced Raman spectroscopy, we also observe a change in Ti site speciation, which occurs via the extraction of mononuclear $[Ti(OSi)_4]$ atoms, and which may be responsible for the changes in observed activity.

Keywords: zeolites; Lewis acid; TS-1; H_2O_2; sustainable chemistry; epoxidation; catalysis

1. Introduction

Over recent decades, remarkable achievements have been observed in the design of Lewis acidic zeolites [1–3]. The biggest breakthrough in this context is titanium silicalite-1 (TS-1), which is a crystalline, porous, MFI-type zeolite doped with a low quantity of framework Ti^{IV} atoms [4]. Possessing active Lewis acid sites, TS-1 has been shown to be an exceptional catalyst for a wide range of oxidation challenges, including olefin epoxidation, aromatic hydroxylation and ketone ammoxidation, amongst others. The unique reactivity of TS-1 is attained when it is reacted at relatively mild conditions with

hydrogen peroxide (H_2O_2), an oxidant with high potential in the area of sustainable chemistry. A pertinent example of this catalysis is the recently commercialised "hydrogen peroxide to propylene oxide" (HPPO) process [5,6]. Despite its industrial exploitation, conventional TS-1 catalyst still exhibits some unfavourable properties. Particularly when employed to perform epoxidation reactions, decreases in epoxide selectivity at high levels of conversion, and the undesirable decomposition of H_2O_2, yielding O_2, are two of its major disadvantages. The second is especially problematic, as unnecessary H_2O_2 decomposition leads both to decreased economic performance through loss of a relative expensive oxidant, and safety concerns associated with the generation of O_2 in the system.

By now, it is widely accepted that the reactivity of TS-1 arises from tetrahedral [$Ti^{IV}(OSi)_4$] sites that are isomorphously substituted into the zeolitic framework, and which may—or may not—be partially hydrolysed [7]. The active sites are proposed to exist in *pseudo*-tetrahedral geometry, comparable to conventional framework atoms, but are believed to be able to expand their co-ordination sphere to six following interaction with solvent molecules and/or the oxidant, due to the flexibility of the MFI framework [7]. Despite this, debate remains regarding the speciation of the Ti active sites, and the nature of the reactive intermediates formed during catalysis, which remains given that *in situ* spectroscopic study is complicated by the presence of water (as by-product), the condensed phase nature of the reaction (solvent spectators), and the lability of Ti-(hydro)peroxo complexes.

Recent work has demonstrated that post-synthetic modification of TS-1 with NH_4HF_2 leads to exciting improvements for aromatic hydroxylation activity and selectivity [8–10]. Despite this, the impact of this treatment on: (i) the active site speciation; and (ii) the activity of TS-1 for other oxidation reactions, particularly epoxidation, remains almost unexplored. In this manuscript we demonstrate the positive impact of NH_4HF_2 treatment on the catalytic activity of TS-1 for olefin epoxidation. Kinetic measurements reveal that following post-synthetic modification, changes in epoxidation activity are observed, and H_2O_2 decomposition activity is almost entirely eliminated, leading to promising breakthroughs in H_2O_2-based selectivity. Through *in situ* spectroscopic study with resonance enhanced Raman spectroscopy, we also observe modifications to the Ti site speciation, which may be responsible for the changes in kinetic behaviour activity.

2. Results and Discussion

2.1. Synthesis of TS-1 and Post-Synthetic Modification with NH_4HF_2

TS-1 was prepared according to a hydrothermal synthesis protocol, and XRD, porosimetry, UV-Vis and FTIR analysis confirm its successful synthesis (ESI Figures S1–S3, Table S1). The post-synthetic modification of calcined TS-1 with NH_4HF_2 and H_2O_2 was performed in an aqueous solution under the conditions optimised by Bianchi and co-workers for 4 h (catalyst henceforth denoted TS-1B) [8–10]. The treatment does not lead to any substantial differences in crystallographic structure, porosity or Ti loading, with each of these parameters remaining constant following NH_4HF_2 treatment. The material is clearly still an MFI type zeolite, and a micropore volume of 0.138 $cm^3 \cdot g^{-1}$ indicates that any potential modification undergone by TS-1 does not change its overall topology or porosity. The Ti loading remains constant, within experimental error, and the Si/Ti molar ratio remains comparable at 43.5 (Table S1).

Clearly, any changes occurring to the material do not involve changes to the crystalline structure, or a major loss of Ti atoms through leaching.

In line with previous research, treatment of TS-1 in NH_4HF_2 does lead to a decrease in the main absorbance band at 210 nm—generally attributed to isomorphously substituted Ti^{IV} atoms [4]—and an increase in absorbance at a wavelength of ±270 nm (ESI Figure S2). Changes are also observed in the FTIR data (ESI Figure S3). The 960 cm^{-1} band—generally attributed to the framework Ti^{IV} atoms [11]—is partially eroded by NH_4HF_2 treatment (spectral intensity normalised to the Si–O–Si overtones of the zeolite lattice), with intensity decreasing by approximately 30% following treatment. According to this provisional characterisation, it may tentatively be attributed that NH_4HF_2 treatment leads to a change to the framework Ti^{IV} atoms. We note that the spectral data presented in Part 1 is in good agreement to the scattered reports of TS-1B in the open literature [8–10].

2.2. Catalytic Studies of Allyl Alcohol Epoxidation

Whilst previous studies of TS-1B have focused upon aromatic hydroxylation [8–10], we chose to investigate the impact of NH_4HF_2 treatment on the epoxidation activity of TS-1. Allyl alcohol was chosen as a model HPPO substrate [6]. Both TS-1 (Figure 1) and TS-1B (Figure 2) were found to be very active catalysts for this reaction. Both catalysts are able to reach full conversion in 120 min or less at the relatively mild reaction temperature of 50 °C. In both cases, glycidol is the main reaction product obtained with >95% selectivity, although 3-methoxy-1,2-propanediol (3M12PD) was also detected, almost fully accounting for the remaining carbon balance. Carbon balances of 95%–98% were always obtained, thus indicated that any other potential by-products below the detectability limit of our analytical protocols were not formed to a major extent. The observation of 3M12PD indicates that ring opening methanolysis of glycidol occurs across the least hindered end of the epoxide. Under a conventional acid catalysed mechanism, 2M13PD would be expected according to Markovnikov's rules. This difference may be due to the active sites in TS-1 catalysing ring opening via a basic mechanism, or may alternatively be a consequence of shape selectivity favouring the linear methoxy-substituted diol over the branched. Although comparable in activity at 50 °C, further kinetic analysis at multiple temperatures reveals distinct differences in the activities of TS-1 and TS-1B.

Initial rate analysis (ESI Figures S4 and S5), calculated from the linear region of the rate plot, and the resulting Arrhenius plot (Figure 3) clearly shows a change to both the temperature dependence and the pre-exponential factor following NH_4HF_2 treatment. The activation energy between 30 and 50 °C is found to increase from 39.1 $kJ \cdot mol^{-1}$ for TS-1, to 53.7 $kJ \cdot mol^{-1}$ for TS-1B. The Arrhenius barrier obtained for TS-1 is found to be in good agreement to previous theoretical studies [12,13]. Although this data indicates that TS-1B is a less active epoxidation catalyst—being less able to reduce the kinetic barrier—this decrease in activity is partially compensated for by an increase in the pre-exponential factor, which increases from 1×10^3 for TS-1, to 2×10^5 for TS-1B. These changes may indicate a modification to the rate-limiting step, and potentially some modifications to the epoxidation pathway.

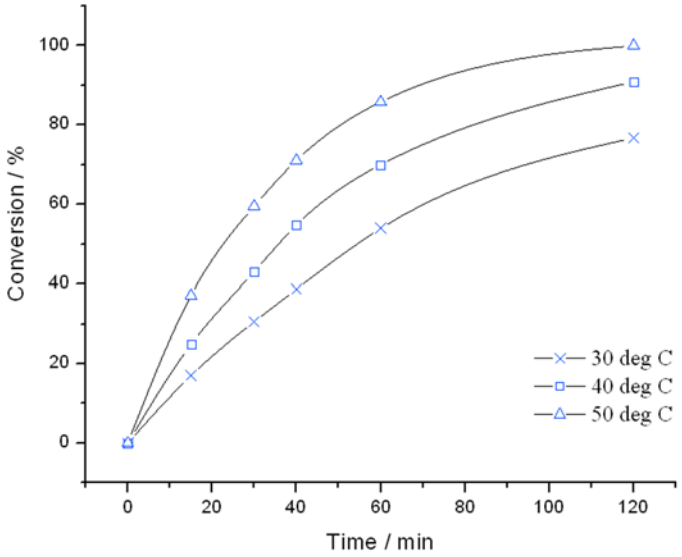

Figure 1. Time online analysis of allyl alcohol epoxidation with TS-1. Reaction conditions: [allyl alcohol] = 0.5 M, [H_2O_2] = 0.25 M, mass TS-1 = 50 mg, various temperatures.

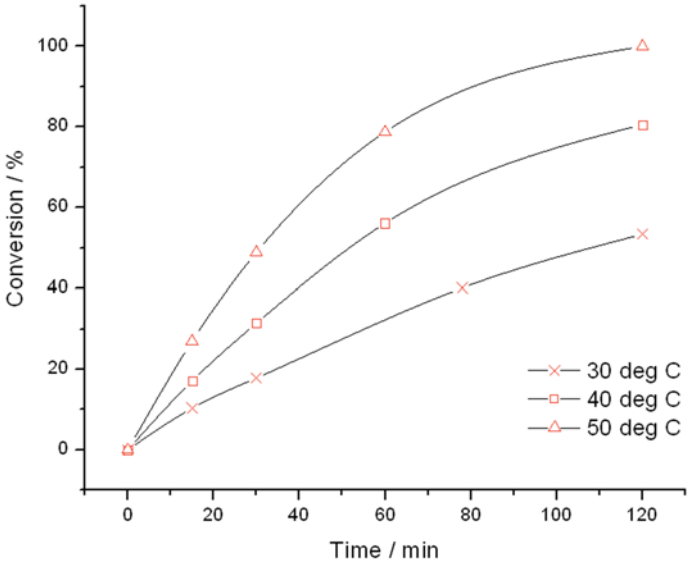

Figure 2. Time online analysis of allyl alcohol epoxidation with TS-1B. Reaction conditions: [allyl alcohol] = 0.5 M, [H_2O_2] = 0.25 M, mass TS-1B = 50 mg, various temperatures. Conversion is calculated according to the initial concentration of H_2O_2 (see experimental section).

Further changes in catalytic performance may also be observed from the conversion *versus* selectivity plots in Figure 4, determined at maximum levels of conversion. Although both catalysts are almost exclusively selective to the main product, glycidol, up to a peroxide conversion level of 80%, it is clear that TS-1B is able to maintain excellent glycidol selectivity even at substantially higher levels of peroxide conversion. Indeed, whilst glycidol selectivity decreases rapidly to ±85% at 95% conversion with TS-1, glycidol selectivity remains well above 90% throughout the conversion range for TS-1B. This increase in selectivity is certainly non-trivial, and would allow the conversion to be held at higher levels. Not only does this avoid the formation of unwanted by-products, and hence decreases separation

issues, but it also leads to higher space-time-yields and the avoidance of unnecessary recycles, which could improve the potential performance of the system on the whole. This improved selectivity may be related to a change in the acid/base character of the active sites, to a change in the way H_2O_2 is activated, or to the better availability of H_2O_2 at very high levels of conversion (See below), limiting the ability of the active sites to catalyse the consecutive reaction.

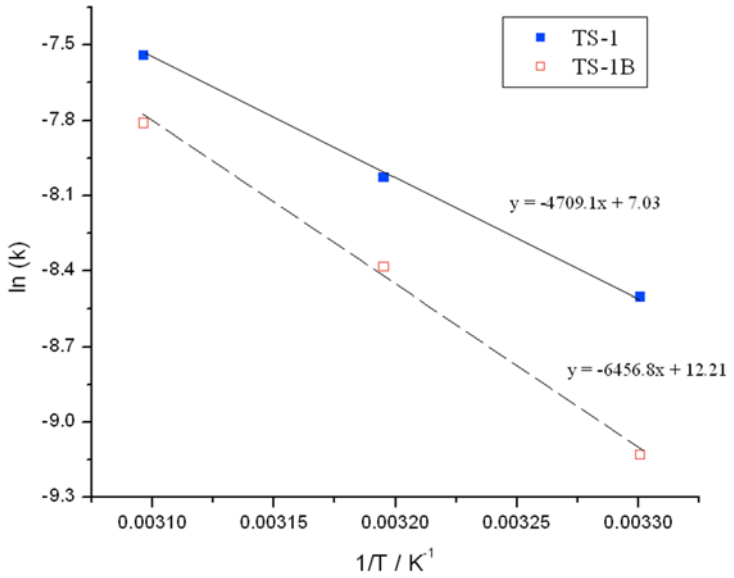

Figure 3. Arrhenius plots obtained for (blue squares) TS-1 and (hollow red squares) TS-1B.

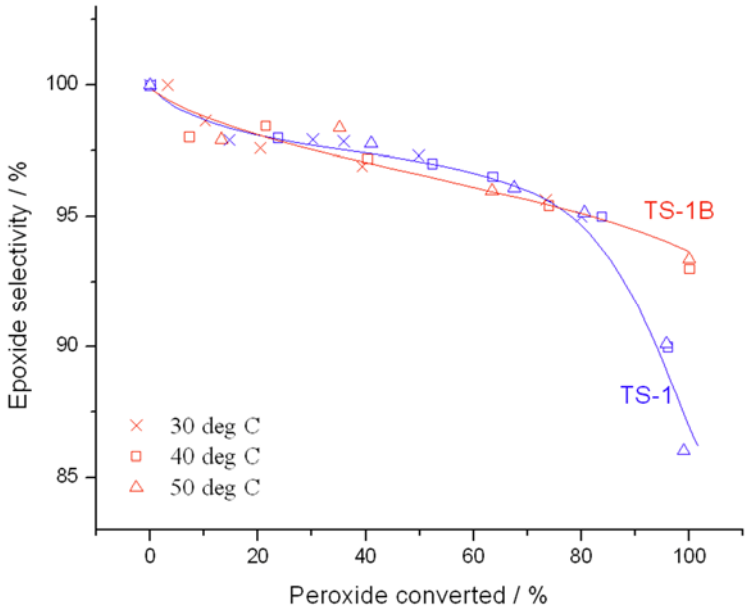

Figure 4. Comparison of selectivity as a function of conversion for (blue) TS-1 and (red) TS-1B. Reaction conditions: [allyl alcohol] = 0.5 M, [H_2O_2] = 0.25 M, mass of catalyst = 50 mg, various temperatures. Conversion is calculated according to the initial concentration of H_2O_2, as a 2:1 olefin:H_2O_2 ratio was employed.

2.3. Catalytic Studies of H_2O_2 Decomposition

To further understand the impact of NH_4HF_2 treatment, we also investigated the ability of TS-1 and TS-1B to catalyse H_2O_2 decomposition. As described above, unwanted H_2O_2 decomposition is clearly disadvantageous, leading to an unwanted loss of expensive oxidant, and potentially increasing safety issues associated. To evaluate the catalytic decomposition of H_2O_2, we performed the epoxidation reaction without the olefin being present, *i.e.*, solvent, catalyst and H_2O_2 concentrations were maintained, but the olefin substrate was absent. The loss of H_2O_2 with time could then be compared to control experiments in the absence of catalyst over the same time period, so as to rule out purely thermal losses (we note here that no thermal losses were observed at temperatures at or below 70 °C).

Both TS-1 and TS-1B are unsurprisingly less reactive for H_2O_2 decomposition than for epoxidation, and longer reaction times are required to induce substantial decomposition. Under reaction conditions identical to the epoxidation reaction, *i.e.*, at 50 °C, neither catalyst decomposes more than 6% of the initial H_2O_2 present in the first 90 min, even in the absence of the olefin. Despite this, clear differences between the decomposition activities of each catalyst can be observed following NH_4HF_2 treatment. Between 40 and 60 °C, TS-1 displays considerable decomposition activity, with conversion reaching a maximum of 53% over TS-1 after 270 min at 60 °C (Figure 5). Whilst these values appear high, we note that decomposition in general is substantially retarded by the co-presence of the olefin, particularly under the reaction conditions employed for epoxidation. The presence of an epoxidisable double bond likely prohibits the Ti-(hydro)peroxo intermediate from liberating O_2 via decomposition or oxidation. Over TS-1, an activation barrier for H_2O_2 decomposition of 70.2 kJ·mol^{-1} was obtained, in excellent agreement to the values found in the open literature (69–72 kJ·mol^{-1}) [14–16].

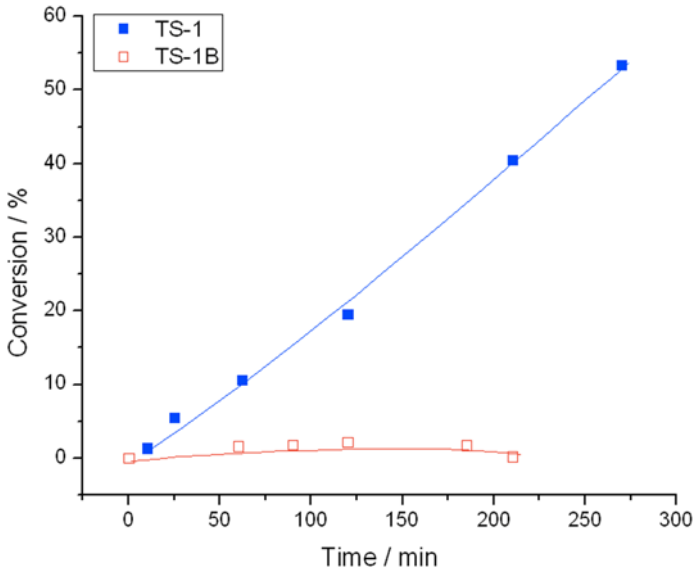

Figure 5. Conversion *versus* time for H_2O_2 decomposition at 60 °C over TS-1 and TS-1B.

In contrast, H_2O_2 decomposition activity is almost completely suppressed following NH_4HF_2 treatment. Indeed, even at 60 °C almost no decomposition is observed following the post-synthetic treatment, with a maximum conversion of 2.1% being observed under the same conditions. The suppression of H_2O_2 decomposition is further exemplified by the Arrhenius plot in Figure 6, following calculation of the

initial rate constants over the linear region of the kinetic plot (ESI Figures S6 and S7). Due to the extremely low reactivity observed over TS-1B we were forced to work at slightly higher temperatures for experiments with this material. Nevertheless, an acceptable Arrhenius barrier of 140 kJ·mol^{-1} was obtained over TS-1B, a two-fold increase in kinetic barrier.

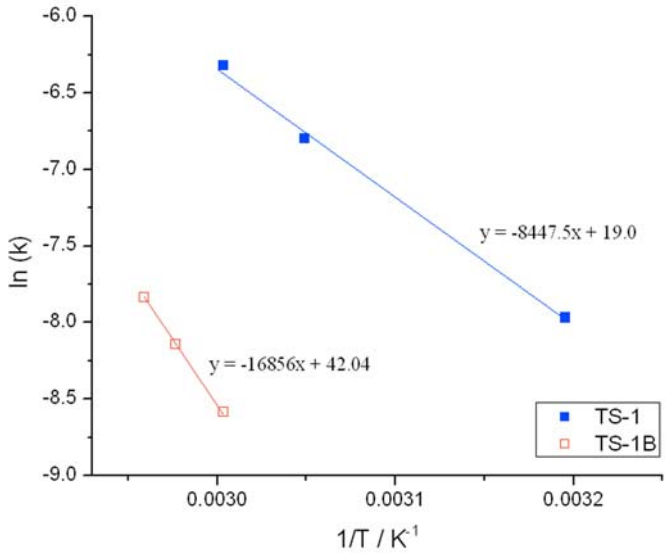

Figure 6. Arrhenius expression for H_2O_2 decomposition over (blue squares) TS-1 and (hollow red squares) TS-1B. Reaction conditions: [H_2O_2] = 0.25 M, mass of catalyst = 50 mg, various temperatures.

2.4. Spectroscopic Studies with in Situ Raman

To account for these interesting effects, particularly the suppression of H_2O_2 decomposition, we considered several possibilities. Although the treatment of various zeolites with NH_4HF_2 has been found to induce some mesopores formation [17], the impact of this was ruled out given the negligible changes observed in the porosimetry data (Table S1). Similarly, changes to the potential acid/base character of TS-1—an important factor in H_2O_2 decomposition chemistry [18]—were also ruled out, based on previous observations that NH_4HF_2 treatment does not change surface acidity (neither Lewis nor Brønsted) to any extent [17]. Fluorine analysis of TS-1B revealed that no residual fluorine remained after treatment (Table S2), and thus changes to the hydrophilicity or polarity of the catalyst based on fluorine are unlikely. Further indication of this was provided through FTIR spectroscopy: Although additional defect sites are indeed observed in TS-1B (ESI Figure S8), these do not obviously change the observed dehydration/rehydration rate compared to TS-1. The potential role of defect sites can also be ruled out given that theoretical studies indicate these would decrease the activation barrier for epoxidation [13], in contrast to our observed kinetics. Whilst ICP analysis also revealed a decrease in trace Fe content following etching (Fe content decreased from 326 to 254 ppm), control measurements investigating the ability of Fe-silicalite-1 to decompose H_2O_2 revealed that the impurity Fe content was not responsible for H_2O_2 decomposition (ESI Table S3). The inability of this MFI material to catalyse H_2O_2 decomposition at a similar Fe loading to that found in TS-1 as impurities clearly indicates that Ti is required for decomposition to proceed, in good agreement with previous studies [18].

Accordingly, we re-focused our attention on spectroscopic study of the Ti active sites with more sensitive spectroscopic techniques. UV-resonance enhanced Raman (UVR) spectroscopy is a particularly promising technique, given its ability to directly probe the Ti active site speciation of each catalyst, improve sensitivity, minimise fluorescence, and selectively probe the different active sites present through the resonance Raman effect [19–21]. The tremendous insight offered by UVR is illustrated in Figure 7. Irradiating TS-1 with a progressively higher energy excitation wavelength allows the LMCT bands of the Ti^{IV} species to be probed, and leads to the identification of Ti^{IV}-specific vibrations more sensitively and selectively. Furthermore, vibrations that are totally undetectable by conventional Raman spectroscopy with IR (Figure 7a) and visible (Figure 7b) sources are also observed due to resonance enhancement effects, although it should be added that species that do not undergo resonance enhancement will not experience improved detectability.

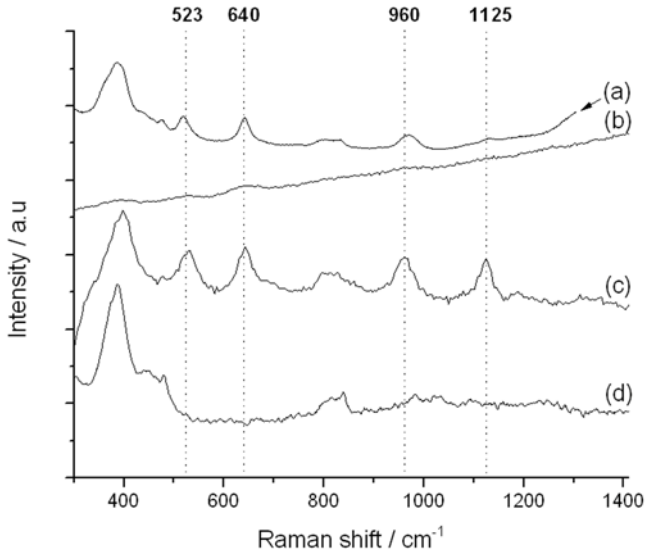

Figure 7. Impact of Raman excitation laser wavelength on Raman spectrum of TS-1. (**a**) TS-1 @785 nm excitation; (**b**) TS-1 @514 nm excitation; (**c**) TS-1 @325 nm excitation; (**d**) silicalite-1 @325 nm excitation.

The 325 nm UV-Raman spectrum of TS-1 is presented in Figure 7c. In addition to the two vibrations related to the zeolite framework at 380 and 800 cm^{-1} (also present in Ti-free silicalite-1, Figure 7d), four vibrations associated with the Ti^{IV} active sites are visible at 523, 640, 960 and 1125 cm^{-1}. The first band (532 cm^{-1}) has previously been assigned to the symmetric stretching vibration of framework Ti–O–Si species [22,23]. Both the 960 and 1125 cm^{-1} bands have also been attributed to the Ti^{IV} active sites of TS-1. These arise from the combination of three asymmetric stretching modes of a tetrahedral $[Ti(OSi)_4]$ unit (960 cm^{-1}), and a totally symmetric stretching mode, *i.e.*, breathing mode, of the same unit (1125 cm^{-1}), respectively [11]. Accordingly, these final two stretches are directly related to the tetrahedrally-coordinated Ti atom present in the $[Ti(OSi)_4]$ active sites. We note that 1125 cm^{-1} band is also known to undergo significant resonance enhancement as the laser is progressively tuned into the LMCT modes, in good agreement with our data (Figure 10) [11]. Accordingly, the 530, 960 and 1125 cm^{-1} UV-Raman bands provide a unique opportunity to monitor the Ti site speciation in TS-1 and TS-1B as a function of post-synthetic modification.

Figure 8 displays the UV-Raman (325 nm) spectra of TS-1 (blue) and TS-1B (red), with the right inset showing the relative intensities of the 960 and 1125 cm^{-1} bands. As can be seen, NH_4HF_2 treatment of TS-1 leads to significant changes in the UV Raman spectrum. The 1125 (inset), 960 (inset), and to a lesser extent the 530 cm^{-1} band (not shown) of TS-1 experience a significant decrease in relative intensity upon NH_4HF_2 treatment. Since the 960 and 1125 cm^{-1} bands have been assigned to stretching modes of a purely tetrahedral [Ti(OSi)$_4$] unit [11], it can be proposed that a general decrease in tetrahedral, framework [Ti(OSi)$_4$] atoms occurs upon post-synthetic modification, *i.e.*, extraction of framework Ti occurs. This is in line with the decrease in the intensity of the 210 nm band in the UV-Vis spectra (ESI Figure S2). Based on the relative intensities of the 960 and 1125 cm^{-1} bands before and after treatment, we estimate the concentration of the original [Ti(OSi)$_4$] atoms have decreased by approximately 25%–50% following NH_4HF_2 treatment, in further agreement to the decreased intensity of the Si–O–Ti band in the FTIR spectra (ESI Figure S3).

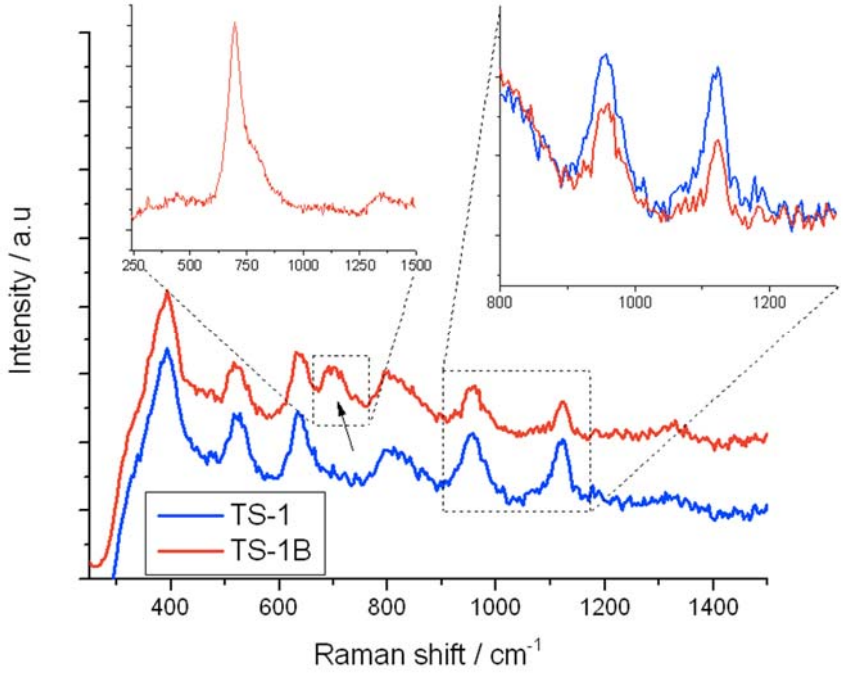

Figure 8. UV-Raman (325 nm) spectra of (blue/bottom) TS-1 and (red/top) TS-1B. The right inset shows the relative intensities of the 960 and 1125 cm^{-1} bands, whilst the left inset shows the intensity of the 695 cm^{-1} band when TS-1B is excited with a 266 nm laser.

Concurrently, a new Raman stretch at 695 cm^{-1} is observed. The generation of a new Raman band is in good agreement to the original UV-Vis data, which demonstrated that a new LMCT band was formed (270 nm) following NH_4HF_2 treatment. Given that this Raman stretch is in the framework, *i.e.*, fingerprint, region of the Raman spectrum, it is likely associated with the Ti^{IV} active sites. However, to verify if this new species was indeed responsible of the absorption band at 270 nm (ESI Figure S2), and is therefore related to the extraction of the [Ti(OSi)$_4$] units, an additional Raman experiment at 266 nm excitation wavelength was performed (Figure 8, left inset). As can be seen, irradiating TS-1B with a 266 nm laser significantly increases the intensity of this stretch by several orders of magnitude. The 266 nm excitation laser overlaps perfectly with the 270 nm absorbance band, thus allowing true

resonance conditions to be met, strongly indicating that this Raman stretch at 695 cm^{-1} is associated with the 270 nm UV-Vis band, and is hence directly proportional to the decrease in $[Ti(OSi)_4]$ atoms. It appears, therefore, that treatment of TS-1 with NH_4HF_2 leads to a general extraction of framework $[Ti(OSi)_4]$ atoms, and the concurrent generation of new Ti sites, which exhibit LMCT bands at ±270 nm, and a Raman stretch at 695 cm^{-1}.

To gain further insight into the active sites present in both TS-1 and TS-1B, we also performed *in situ* UV-Raman spectroscopy (Figure 9), where both TS-1 and TS-1B were treated with H_2O_2. In good agreement to previous *in situ* Raman studies of TS-1, complete elimination of the 960 and 1125 cm^{-1} bands are observed upon treatment of TS-1 with H_2O_2 [24,25]. Given that these bands are associated with various stretching and breathing modes of the $[Ti(OSi)_4]$ tetrahedron, the total loss of these stretches can be attributed to the change in geometry (from tetrahedral to octahedral) that occurs upon the formation of the relevant Ti-(hydro)peroxo species. We note that the original spectrum can be restored by a heat treatment at 90 °C, and may even partially be restored by extended scanning under the Raman beam.

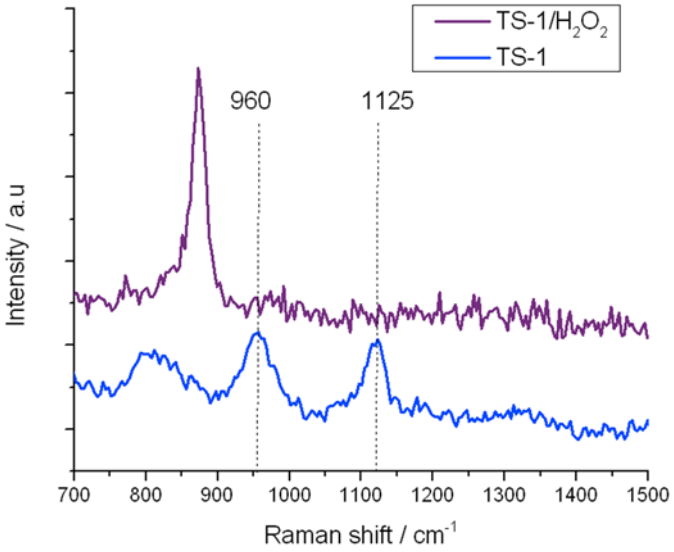

Figure 9. *In situ* UV-Raman (325 nm) spectra of (blue) TS-1 and (purple) TS-1 treated with H_2O_2.

Similarly, the residual 960 and 1125 cm^{-1} stretches in TS-1B are also eliminated upon treatment with H_2O_2, confirming that at least some of the original active site remains following NH_4HF_2 treatment. However, it is also notable that the 695 cm^{-1} band, which has been attributed to the new 270 nm UV-Vis absorbance band, is also eliminated from the Raman spectrum upon coordination of H_2O_2. The total loss of this Raman band confirms (i) that this Raman mode arises from a species whose vibrational signature is destroyed upon coordination of H_2O_2; and (ii) that the new active site formed following NH_4HF_2 treatment reacts with H_2O_2, indicating that this species also provides a route toward H_2O_2 activation. From the characterization data obtained thus far, we assign this change in Ti speciation to the extraction of framework $[Ti(OSi)_4]$ atoms, and to the concurrent generation of new active sites. Given that a redistribution of Ti from one T-site to another would not change the intensity of the breathing mode of the $[Ti(OSi)_4]$ atoms at 1125 cm^{-1}, it is likely that the new active sites are located in extra-framework positions of the zeolite.

At this time, we are not able to conclusively attribute the modified kinetic behaviour to the generation of extra-framework Ti species. Yet, the *in situ* UV-Raman data and the absence of any other contributing factors (see above) strongly suggest that these factors are related. We consider there to be two potential ways that the extraction of framework Ti could lead to such pronounced changes. The first possibility is that NH_4HF_2 treatment removes a particularly non-selective framework [$Ti(OSi)_4$] site, responsible for both epoxidation and undesirable decomposition. Alternatively, the extraction of framework Ti could result in the formation of active, extra-framework Ti complexes, which may provide an alternative pathway for H_2O_2 activation. In light of the *in situ* UV-Raman analysis (Figure 10), we favour the latter. Given the narrow FWHM observed in the UV-Vis spectrum of TS-1B (ESI Figure S2), and the generation of only one new Raman active mode, we hypothesise that any extra-framework complex must be either mononuclear, or of low nuclearity (*cf.* dimeric). Although reports suggest mononuclear, extra-framework Ti to be inactive for epoxidation [26], several recent reports have highlighted the potential for two concerted Ti sites to catalyse epoxidation reactions: Kortz *et al.* demonstrated that a polyoxometallate containing a unique di-titanium centre ($[Ti_2(OH)_2As_2W_{19}O_{67}(H_2O)]$ [8]) is able to activate $H_2O_2$for epoxidation catalysis [27], and the barrier calculated for H_2O_2 activation over a model Ti-dimer complex was found to be 53.5 $kJ \cdot mol^{-1}$ by Lundin *et al.* [28] This value is especially close to the experimental barrier of TS-1B. Definitive identification of the new active sites, and their potential role in the epoxidation/decomposition process, will require further (*in situ*) spectroscopic study with complimentary techniques, such as X-ray Absorption spectroscopy and computational methodologies. These additional spectroscopic, computational and kinetic studies remain the focus of our on-going work.

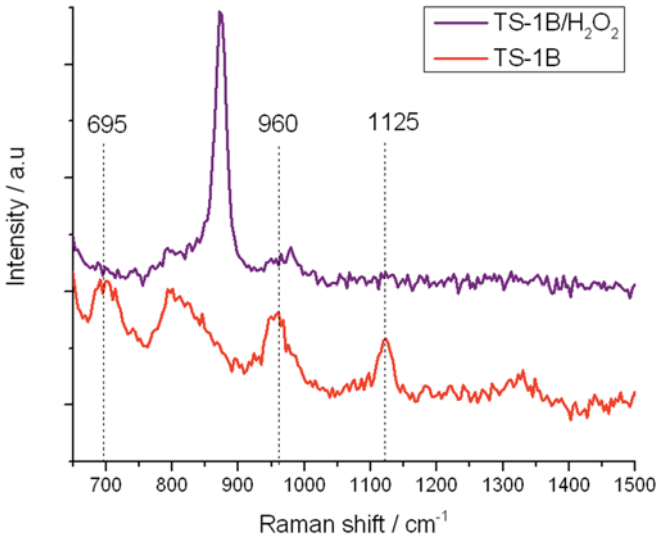

Figure 10. *In situ* UV-Raman (325 nm) spectra of (red) TS-1B and (purple) TS-1B treated with H_2O_2.

3. Experimental Section

3.1. Catalyst Synthesis and Pre-Treatment

TS-1 was prepared according to a method described elsewhere [29]. TS-1B was prepared as follows. TS-1 (4 g) was suspended in an aqueous solution (80 mL) containing NH_4HF_2 (120 mg) and H_2O_2

(50 wt. %, 3.2 mL). The slurry was stirred for 4 h at 80 °C, prior to filtration. The sample was finally dried overnight (110 °C, 16 h).

3.2. Catalyst Characterization

Powder X-ray diffraction was performed on a PANalytical X'PertPRO X-ray diffractometer (PANalytical, Almelo, the Netherlands), with a CuKα radiation source (40 kV and 30 mA). Diffraction patterns were recorded between 6° and 55°. FTIR spectroscopy was performed on a Bruker Tensor spectrometer (Bruker Corporation, MA, USA) over a range of 4000–650 cm^{-1} at a resolution of 2 cm^{-1}. UV-Vis analysis was performed on an Agilent Cary 4000 UV-Visible Spectrophotometer (Agilent Technologies, CA, USA) in Diffuse Reflectance mode. Samples were measured between 190 and 800 nm at 600 $nm \cdot min^{-1}$ scan rate. Ti content and Si/Ti molar ratios were determined by EDX. Specific surface area was determined from nitrogen adsorption using the BET equation, and microporous volume was determined from nitrogen adsorption isotherms using the *t*-plot method. Porosimetry measurements were performed on a Quantachrome Autosorb (Quantachrome, FL, USA), and samples were degassed prior to use (275 °C, 3h). Adsorption isotherms were obtained at 77 K. UV-Raman spectroscopy was performed on a Renishaw inVia spectrometer (Renishaw plc, Gloucestershire, UK) equipped with laser lines at 785, 514, 325 and 266 nm. Laser power was kept at or below 10 mW for solid powders, and at or below 2 mW for *in situ* measurements with H_2O_2.

3.3. Kinetic Evaluation and Analytical Methods

Allyl alcohol epoxidation was performed in a 100 mL round bottom flask equipped with a reflux condenser, thermostatically controlled by immersion in a silicon oil bath. The vessel was first charged with a 10 mL solution of allyl alcohol in methanol (0.5 M), which also contained an internal standard (biphenyl, 0.025M). The desired amount of catalyst (50 mg) was also added. The mixture was subsequently heated to the desired temperature (stated in the manuscript, all temperatures correspond to the oil temperature outside the reactor), and the reaction was initiated by addition of an appropriate amount of H_2O_2 (0.25 M, corresponding to a 1:2 H_2O_2:olefin ratio). The solution was stirred at ±750 rpm with an oval magnetic stirrer bar. Aliquots of reaction solution were taken periodically for analysis, and were centrifuged prior to injection into a GC (Agilent 7820 (Agilent Technologies, CA, USA), 25 m CP-Wax 52 CB column). Reactants were quantified against the biphenyl internal standard. Conversion was calculated as follows: Conversion = Σ[products, M]/$[H_2O_2]_0 \times 100$. All chemicals were purchased from Sigma-Aldrich (St. Louis, MO, USA).

4. Conclusions

Titanium silicalite-1 is a uniquely active catalyst for a range of commercial scale oxidation reactions. In this manuscript, we demonstrate that treatment of TS-1 with NH_4HF_2 leads to a change in Ti site speciation. Through UV-Vis, FTIR and UV-resonance enhanced Raman spectroscopy, we interpret this change as being related to the extraction of mononuclear $[Ti(OSi)_4]$ atoms from the zeolite framework, and the generation of new active Ti species that are present in extra-framework sites of the structure. These new active sites may be responsible both for the changes in epoxidation catalysis

observed (increased selectivity, modified temperature dependence), and also for significant improvements in H_2O_2-based selectivity, as non-selective H_2O_2 decomposition is found to be drastically decreased following post-synthetic treatment of TS-1 with NH_4HF_2.

Acknowledgments

C.H. gratefully appreciates the support of The Royal Society for the provision of a University Research Fellowship (UF140207) and additional research funding (RG140754).

Author Contributions

C.H. Conceived and designed the experiments and guided the research. G.T. and C.H. performed characterization and catalytic studies. C.H. performed the Raman measurements. Both authors contributed to the writing of the manuscript.

Conflicts of Interest

The authors declare no conflict of interest.

References

1. Corma, A.; Garcia, H. Lewis Acids as Catalysts in Oxidation Reactions: From Homogeneous to Heterogeneous Systems. *Chem. Rev.* **2002**, *102*, 3837–3892.
2. Moliner, M. State of the Art of Lewis Acid-Containing Zeolites: Lessons From Fine Chemistry to New Biomass Transformation Processes. *Dalton Trans.* **2014**, *43*, 4197–4208.
3. Dapsens, P.Y.; Mondelli, C.; Perez-Ramirez, J. Design of Lewis-acid centres in zeolitic matrices for the conversion of renewables. *Chem. Soc. Rev.* **2015**, *44*, 7025–7043.
4. Ratnasamy, P.; Srinivas, D.; Knözinger, H. Active Sites and Reactive Intermediates in Titanium Silicate Molecular Sieves. *Adv. Catal.* **2004**, *48*, 1–169.
5. Cavani, F.; Teles, J.H. Sustainability in Catalytic Oxidation: An Alternative Approach or Structural Evolution? *ChemSusChem* **2009**, *2*, 508–534.
6. Cavani, F. Catalytic Selective Oxidation: The Forefront in the Challenge for a More Sustainable Chemical Industry. *Catal. Today* **2010**, *157*, 8–15.
7. Bordiga, S.; Bonino, F.; Damin, A.; Lamberti, C. Reactivity of Ti(IV) species hosted in TS-1 towards H_2O_2-H_2O Solutions investigated by ab initio cluster and periodic approaches combined with experimental XANES and EXAFS data: a review and new highlights. *Phys. Chem. Chem. Phys.* **2007**, *9*, 4854–4878.
8. Balducci, L.; Bianchi, D.; Bortolo, R.; D'Aloisio, R.; Ricci, M.; Tassinari, R.; Ungarelli, R. Direct Oxidation of Benzene to Phenol with Hydrogen Peroxide over a Modified Titanium Silicalite. *Angew. Chem. Int. Ed.* **2003**, *42*, 4937–4940.
9. Bianchi, D.; D'Aloisio, R.; Bortolo, R.; Ricci, M. Oxidation of Mono- and Bicyclic Aromatic Compounds with Hydrogen Peroxide Catalyzed by Titanium Silicalites TS-1 and TS-1B. *Appl. Catal. A* **2007**, *327*, 295–299.

10. Bianchi, D.; Balducci, L.; Bortolo, R.; D'Aloisio, R.; Ricci, M.; Spanò, G.; Tassinari, R.; Tonini, C.; Ungarelli, R. Oxidation of Benzene to Phenol with Hydrogen Peroxide Catalyzed by a Modified Titanium Silicalite (TS-1B). *Adv. Synth. Catal.* **2007**, *349*, 979–986.
11. Ricchiardi, G.; Damin, A.; Bordiga, S.; Lamberti, C.; Spanò, G.; Rivetti, F.; Zecchina, A. Vibrational Structure of Titanium Silicate Catalysts. A Spectroscopic and Theoretical Study. *J. Am. Chem. Soc.* **2001**, *123*, 11409–11419.
12. Wells, D.H., Jr.; Joshi, A.M.; Delgass, N.; Thomson, K.T. A Quantum Chemical Study of Comparison of Various Propylene Epoxidation Mechanisms Using H_2O_2 and TS-1 Catalyst. *J. Phys. Chem. B* **2006**, *110*, 14627–14639.
13. Wells, D.H., Jr.; Delgass, N.; Thomson, K.T. Evidence of Defect-Promoted Reactivity for Epoxidation of Propylene in Titanosilicate (TS-1) Catalysts: A DFT Study. *J. Am. Chem. Soc.* **2004**, *126*, 2956–2962.
14. Wang, L.; Wang, Y.; Wu, G.; Feng, W.; Zhang, T.; Yang, R.; Jin, X.; Shi, H. A Novel Kinetics Study on H_2O_2 Decomposition in the Propylene Epoxidation System in a Fixed Bed Reactor. *Int. J. Chem. React. Eng.* **2013**, *11*, 265–269.
15. Potekhin, V.V.; Kulikova, V.A.; Kochina, E.G.; Potekhin, V.M. Decomposition of Hydrogen Peroxide in Protic and Polar Aprotic Solvents on TS-1 Heterogeneous Catalyst. *Russ. J. Appl. Chem.* **2011**, *84*, 1195–1200.
16. Shan, Z.C.; Lu, Z.D.; Wang, L.; Zhou, C.; Ren, L.M.; Zhang, L.; Meng, X.J.; Ma, S.J.; Xiao, F.S. Stable Bulky Particles Formed by TS-1 Zeolite Nanocrystals in the Presence of H_2O_2. *ChemCatChem* **2010**, *2*, 407–412.
17. Qin, Z.; Lakiss, L.; Gilson, J.-P.; Thomas, K.; Goupil, J.-M.; Fernandez, C.; Valtchev, V. Chemical Equilibrium Controlled Etching of MFI-Type Zeolite and Its Influence on Zeolite Structure, Acidity, and Catalytic Activity. *Chem. Mater.* **2013**, *25*, 2759–2766.
18. Yoon, C.W.; Hirsekorn, K.F.; Neidig, M.L.; Yang, X.; Tilley, T.D. Mechanism of the Decomposition of Aqueous Hydrogen Peroxide over Heterogeneous TiSBA15 and TS-1 Selective Oxidation Catalysts: Insights from Spectroscopic and Density Functional Theory Studies. *ACS Catal.* **2011**, *1*, 1665–1678.
19. Kim, H.; Kosuda, K.M.; van Duyne, R.P.; Stair, P.C. Resonance Raman and Surface- and Tip-enhanced Raman Spectroscopy Methods to Study Solid Catalysts and Heterogeneous Catalytic Reactions. *Chem. Soc. Rev*. **2010**, *39*, 4820–4844.
20. Fan, F.; Feng, Z.; Li, C. UV Raman Spectroscopic Study on the Synthesis Mechanism and Assembly of Molecular Sieves. *Chem. Soc. Rev*. **2010**, *39*, 4794–4801.
21. Fan, F.; Feng, Z.; Li, C. UV Raman Spectroscopic Studies on Active Sites and Synthesis Mechanisms of Transition Metal-Containing Microporous and Mesoporous Materials. *Acc. Chem. Res.* **2010**, *43*, 378–387.
22. Guo, Q.; Sun, K.; Feng, Z.; Li, G.; Guo, M.; Fan, F.; Li, C. A Thorough Investigation of the Active Titanium Species in TS-1 Zeolite by In Situ UV Resonance Raman Spectroscopy. *Chem. Eur. J.* **2012**, *18*, 13854–13860.
23. Li, C.; Xiong, G.; Xin, Q.; Liu, J.; Ying, P.; Feng, Z.; Li, J.; Yang, W.; Wang, Y.; Wang, G.; *et al*. UV Resonance Raman Spectroscopic Identification of Titanium Atoms in the Framework of TS-1 Zeolite. *Angew. Chem. Int. Ed.* **1999**, *38*, 2220–2221.

24. Bordiga, S.; Damin, A.; Bonino, F.; Ricchiardi, G.; Zecchina, A.; Tagliapietra, R.; Lamberti, C. Resonance Raman Effects in TS-1: the Structure of Ti(IV) Species and Reactivity Towards H_2O, NH_3 and H_2O_2: an in situ Study. *Phys. Chem. Chem. Phys.* **2003**, *5*, 4390–4393.
25. Bordiga, S.; Damin, A.; Bonino, F.; Ricchiardi, G.; Lamberti, C.; Zecchina, A. The Structure of the Peroxo Species in the TS-1 Catalyst as Investigated by Resonant Raman Spectroscopy. *Angew. Chem. Int. Ed.* **2002**, *41*, 4734–4737.
26. Li, G.; Wang, X.; Guo, X.; Liu, S.; Zhao, Z.; Bao, X.; Lin, L. Titanium Species in TS-1 Prepared by Hydrothermal Method. *Mat. Chem. Phys.* **2001**, *71*, 195–201.
27. Hussain, F.; Bassil, B.S.; Kortz, U.; Kholdeeva, O.A.; Timofeeva, M.N.; de Oliveira, P.; Keita, B.; Nadjo, L. Di-titanium-containing 19-tungstodiarsenate (III) $[Ti_2(OH)_2As_2W_{19}O_{67}(H_2O)]^{8-}$: Synthesis, structure, electrochemistry, and oxidation catalysis. *Chem. Eur. J.* **2007**, *13*, 4733–4742.
28. Lundin, A.; Panas, I.; Ahlberg, E. Quantum Chemical Modeling of Propene and Butene Epoxidation with Hydrogen Peroxide. *J. Phys. Chem. A* **2009**, *113*, 282–290.
29. Hammond, C.; Dimitratos, N.; Jenkins, R.L.; Lopez-Sanchez, J.A.; Kondrat, S.A.; Rahim, M.H.A.; Forde, M.M.; Thetford, A.; Taylor, S.; Hagen, H.; *et al*. Elucidation and Evolution of the Active Component within Cu/Fe/ZSM-5 for Catalytic Methane Oxidation: From Synthesis to Catalysis. *ACS Catal.* **2013**, *3*, 689–699.